International Journal of Engineering Inventions
e-ISSN: 2278-7461, p-ISSN: 2319-6491
Volume 15, Issue 5 [May 2026] PP: 115-122

Cloud Detection for FY-4B/AGRI Data Based on the Fmask Algorithm

Jiayu Liu
Department of Surveying and Mapping Engineering, School of Surveying and Land Information Engineering, Henan Polytechnic University, Jiaozuo, Henan, China
Corresponding Author: Jiayu Liu.

ABSTRACT: *Cloud cover is a key factor that leads to information loss in remote sensing imagery, reduces data usability, and affects the accuracy of subsequent quantitative processing. The Advanced Geostationary Radiation Imager (AGRI) onboard China's new-generation geostationary meteorological satellite FY-4B provides multispectral Earth observations with high temporal resolution. Developing an automated and high-precision cloud detection method suitable for AGRI data is of great significance. Based on the logic of the Fmask algorithm, this study constructs a cloud detection method for AGRI data at 4 km spatial resolution. The algorithm is improved with respect to the band configuration of AGRI and the characteristics of geostationary observations. Given the absence of the 0.55μm green band, the whiteness index is reconstructed using the blue and red bands. The spectral thresholds and discrimination conditions in the basic test, HOT test, rock test, and water test are optimized. Cloud probability models are established separately for land and water, integrating temperature probability, brightness probability, and spectral variability probability to achieve pixel-level cloud identification. FY-4B/AGRI images covering different geographical regions and full-disk scales are selected for validation, and the detection results are visually compared with false-color composite images. The results show that the improved algorithm effectively identifies thick clouds, thin clouds, and fragmented clouds, with clear cloud boundaries and low false detection rates over both land and sea backgrounds. The full-disk detection results are highly consistent with visual interpretation. This study provides a reliable cloud detection method for FY-4B/AGRI data, supporting subsequent quantitative remote sensing retrieval and operational meteorological applications.*

Date of Submission: 07-05-2026 Date of acceptance: 17-05-2026

I. INTRODUCTION

Clouds play an important role in the Earth's climate system, affecting multiple aspects including radiative transfer, the water cycle, and climate change[1-3]. According to statistics from the International Satellite Cloud Climatology Project (ISCCP), the global annual mean cloud cover is approximately 66%[4,5]. Cloud cover not only directly leads to information loss in remote sensing imagery and reduces data usability, but also affects the accuracy of subsequent quantitative processing, such as land cover classification and parameter retrieval[6-8]. Therefore, accurate cloud detection has become a critical step in remote sensing image processing. Developing high-precision cloud detection algorithms adapted to different sensor characteristics is of great significance for improving the overall quality of remote sensing data products.

Based on the characteristics of clouds—high reflectance and low temperature—researchers have developed a variety of technical methods. Early cloud detection studies were mainly based on spectral thresholds, where discrimination conditions were set by analyzing the spectral properties of different bands. Among these, the Automatic Cloud Cover Assessment (ACCA) and the Function of mask (Fmask) methods have become the most representative approaches based on spectral thresholds[9,10]. The Fmask algorithm integrates top-of-atmosphere (TOA) reflectance and brightness temperature, calculates probabilities based on the physical properties of clouds, and can simultaneously detect cloud shadows and snow. Owing to its clear physical basis and strong interpretability, Fmask has been widely applied to Landsat and Sentinel-2 data and has undergone continuous improvement[11-13]. However, methods based on spectral thresholds require a sufficient number of spectral bands and have limited generalization ability over complex underlying surfaces[14].

In addition, machine learning methods have recently been introduced into cloud detection tasks for multispectral remote sensing data. By training classifiers such as support vector machines[15] and random forests[16], these methods automatically extract the spectral and spatial features of clouds and cloud shadows, thereby improving detection performance in complex scenes[17,18]. For FY-4A/AGRI data, Guo Xuexing et al. developed a classifier based on the naive Bayes method, enabling all-time cloud detection using only infrared

channels[19]. On this basis, deep learning methods have further improved the accuracy and robustness of cloud detection. For example, the MSCFF method proposed by Li et al. achieves high-precision detection across different sensor images through multi-scale feature fusion[20]. However, although machine learning and deep learning methods outperform traditional approaches in terms of detection performance, they still rely heavily on large-scale annotated samples and high computational resources. When facing complex scenes, such methods may suffer from reduced accuracy[21].

As China's new-generation geostationary meteorological satellite, FY-4B is equipped with the Advanced Geosynchronous Radiation Imager (AGRI), which provides multispectral Earth observations with high temporal resolution, supporting real-time meteorological monitoring and climate research[22]. Developing an automated and high-precision cloud detection method suitable for FY-4B/AGRI data is of great importance for climate change monitoring, land surface parameter retrieval, and refined meteorological services. Based on the detection logic of the Fmask algorithm, this study constructs a cloud detection algorithm applicable to FY-4B/AGRI data at 4 km spatial resolution.

II. DATA DESCRIPTION

FY-4 is China's second-generation geostationary meteorological satellite series developed independently, of which FY-4B was launched in June 2021. As the core payload of the FY-4 series, the Advanced Geosynchronous Radiation Imager (AGRI) has 15 spectral channels covering the visible to longwave infrared range from 0.45 to 13.60μm[23]. Table(1) lists the key band parameters and corresponding spatial resolutions of the Landsat and AGRI sensors that are applicable to the Fmask algorithm. A comparative analysis shows that although most of the visible to shortwave infrared bands of AGRI correspond to those of MODIS, some differences remain. For example, AGRI lacks the 0.55μm green band, and its spatial resolution is generally lower than that of Landsat. Therefore, the Fmask algorithm needs to be adapted to the band configuration of the FY-4B/AGRI sensor and the observation characteristics of geostationary satellites to ensure its suitability for AGRI data.

Table(1) Comparison of spectral band configurations between Landsat TM and FY-4B AGRI

	Landsat TM			FY4B AGRI	
Band number	Resolution/m	Wavelength/μm	Band number	Resolution/m	Wavelength/μm
1	30	0.45～0.52	1	1000	0.45～0.49
2	30	0.52～0.60			
3	30	0.63～0.69	2	500	0.55～0.75
4	30	0.76～0.90	3	1000	0.75～0.90
5	30	1.55～1.75	5	2000	1.58～1.64
6	120	10.40～12.50	14	4000	11.5～12.50
7	30	2.08～2.35	6	2000	2.10～2.35

III. CLOUD DETECTION ALGORITHM

The Fmask cloud detection algorithm is based on the physical properties of clouds and achieves automated cloud detection using spectral threshold conditions. The algorithm exploits the "white" appearance of clouds, resulting from their approximately equal reflectance in the visible bands, as well as their low temperature due to their higher spatial position. By applying predefined thresholds, non-cloud pixels are progressively excluded. In addition, the algorithm incorporates multispectral indices such as the Normalized Difference Vegetation Index (NDVI) and the Normalized Difference Snow Index (NDSI) for comprehensive cloud identification[10,11].

POTENTIAL CLOUD PIXEL IDENTIFICATION

The identification of potential cloud pixels is achieved through a series of spectral threshold tests, aiming to preliminarily screen pixels that meet the physical characteristics of clouds. All tests are based on top-of-atmosphere (TOA) reflectance and brightness temperature data. The specific steps are as follows:

(1) Basic Test

The basic test takes advantage of the high reflectance of clouds in the visible bands and their low temperature in the thermal infrared band. It sets initial discrimination conditions as: Band6 TOA reflectance greater than 0.05, and Band14 brightness temperature lower than 27°C. Since the reflectance of clouds varies little across different bands, their Normalized Difference Vegetation Index (NDVI) and Normalized Difference

Snow Index (NDSI) are usually close to zero, whereas healthy vegetation has a high NDVI and snow cover has a high NDSI. To reduce the interference of vegetation and snow on cloud identification, the algorithm further imposes threshold conditions of NDSI < 0.8 and NDVI < 0.8, in order to identify as many potential cloud pixels as possible. The test formula is as follows:

$$\begin{aligned} \text{BasicTest} = {} & Band6 > 0.05 \text{ and } BT < 27 and \\ & NDSI < 0.8 \text{ and } NDVI < 0.8 \\ \text{Where,} & \\ \text{NDSI} = {} & (Band2 - Band5)/(Band\ 2 + Band5) \\ \text{NDVI} = {} & (Band3 - Band2)/(Band\ 3 + Band2). \end{aligned} \tag{1}$$

(2) Whiteness Test

The whiteness test is based on the characteristic that clouds exhibit a white appearance due to their smooth reflectance variation across the visible bands. It constructs a whiteness index by calculating the ratio of the absolute difference between visible bands to the overall brightness, which is then used to identify cloud pixels. The original Landsat Fmask algorithm uses the 0.55μm green band for this calculation. However, since the FY-4B/AGRI data lack this band, this study uses Band1 (blue) and Band2 (red) as substitutes. By taking the ratio of the band difference to the average value of the visible bands as the whiteness index and setting the threshold to 0.75, pixels that have high reflectance in the visible bands but are not sufficiently "white" can be effectively excluded. It should be noted that this test may still include some pixels of bare soil, sand, snow, and ice, as these surfaces also exhibit approximately equal reflectance in the visible bands. The specific formula is as follows:

$$\text{MeanVis} = (Band1 + Band2)/2$$

$$\text{Whiteness Test} = \sum_{i=1}^{2} |(Band\ i - Mean\ Vis)/Mean\ Vis|. \tag{2}$$

(3) HOT Test

The HOT (Haze Optimized Transformation) test is based on the high correlation of surface reflectance in the visible bands under clear-sky conditions. When haze or thin clouds are present in the atmosphere, the spectral responses of the blue and red bands differ significantly, manifesting as a deviation of pixels from the clear-sky line in the blue-red scatter plot. Pixels affected by clouds typically shift downward and to the right, with the shift increasing as cloud thickness increases. By quantifying this shift, the HOT test can effectively identify clouds and thick aerosols. However, this test may still misclassify some high-reflectance surfaces (such as rocks, turbid water, snow, and ice) as clouds. The specific formula is as follows:

$$\text{HOT Test} = Band1 - 0.5 \times Band2 - 0.08. \tag{3}$$

(4) Rock Test

The rock test is based on the characteristic that cloud reflectance in Band5 is lower than that in Band3, whereas the opposite is true for bright land surfaces. Although the traditional threshold (ratio greater than 1) can exclude bright surfaces, it tends to miss thin clouds. Based on a sensitivity analysis using a global cloud reference dataset, Fmask lowers the threshold to 0.75, thereby retaining thin clouds while effectively separating clouds from bright rocks. The specific formula is as follows

$$\text{Rock Test} = \frac{Band3}{Band5} > 0.75. \tag{4}$$

(5) Water Test

The Fmask algorithm classifies pixels into water and land through the water test. Water bodies typically exhibit low reflectance in the near-infrared (NIR) band, appearing dark, while land surfaces have higher reflectance. The test combines NIR reflectance and NDVI for discrimination, with the following criteria: NDVI < 0.15 and Band3 reflectance < 0.08, or NDVI < 0.01 and Band3 reflectance < 0.11. The specific formula is as follows:

$$\begin{aligned} \text{Water Test} = {} & (NDVI < 0.01 \text{ and } Band3 < 0.11) \text{ or} \\ & (NDVI < 0.15 \text{ and } Band3 < 0.08). \end{aligned} \tag{5}$$

When a pixel simultaneously satisfies the basic test, whiteness test, HOT test, and rock test, it is identified as a potential cloud pixel (PCP). The first pass of detection is designed to overestimate cloud cover. If the proportion of PCPs exceeds 99.9%, the cloud mask is output directly; otherwise, the algorithm proceeds to the second pass.

POTENTIAL CLOUD LAYER

Due to significant differences in temperature distribution and reflectance range between land and water, the Fmask algorithm constructs separate cloud probability models for each surface type. Clear-sky water pixels are identified using the water test and Band6 reflectance (less than 0.03). Clear-sky land pixels are determined as non-PCP and non-water pixels. Based on these, the algorithm combines water temperature probability with brightness probability for water pixels, and land temperature probability with variability probability for land pixels, calculating the overall cloud probability on a pixel-by-pixel basis.

To exclude the influence of atmospheric effects that may lower water temperature, the clear-sky water temperature (T_{water}) is taken as the 82.5th percentile of the brightness temperatures of clear-sky water pixels. Based on the physical property that the cloud probability is high when the brightness temperature is 4°C lower than the surface temperature, the water temperature probability is normalized using the ratio of the temperature difference to 4°C. The specific formula is as follows:

$$\text{wTemperature}_{\text{Prob}} = \frac{T_{water} - BT}{4}. \tag{6}$$

The reflectance of clear-sky water in Band5 is typically lower than 0.05, while turbid or shallow water areas can have reflectances as high as 0.11. The presence of clouds significantly increases the reflectance in this band. Therefore, the Fmask algorithm normalizes the Band5 reflectance using Equation (7) to calculate the brightness probability for water.

$$\text{Brightness\_Prob} = \min(Band5, 0.11)/0.11. \tag{7}$$

The water cloud probability (wCloud_Prob) is calculated as the product of the water temperature probability and the brightness probability. For cold pixels, the contribution of the temperature probability is generally more significant due to its wider dynamic range. By combining the temperature and brightness probabilities, bright water pixels (e.g., shallow or turbid water) and cold water pixels (e.g., high-altitude water bodies) can be effectively excluded: when either probability is close to zero, the water cloud probability approaches zero regardless of the value of the other probability. The specific formula is as follows:

$$\text{wCloud}_{\text{Prob}} = wTemperature_{Prob} * Brightness_{Prob}. \tag{8}$$

The upper and lower bounds of the clear-sky land temperature are taken as the 82.5th and 17.5th percentiles, respectively, of the brightness temperatures of clear-sky land pixels. If the brightness temperature of a pixel is 4°C lower than the lower bound, the cloud probability is high; if it is 4°C higher than the upper bound, the pixel is most likely clear-sky. Based on this temperature interval, the land temperature probability is calculated using a normalization method. The specific formula is as follows:

$$\text{lTemperature\_Prob} = \frac{\left(T_{high} + 4 - BT\right)}{\left(T_{high} + 4 - (T_{low} - 4)\right)}. \tag{9}$$

Due to the high variability in reflectance of land pixels, brightness probability is not suitable for cloud detection over land. Therefore, the Fmask algorithm introduces three indices—whiteness, NDVI, and NDSI—to characterize the spectral differences within the visible bands, between the near-infrared and visible bands, and between the shortwave infrared and visible bands, respectively. Clouds typically exhibit low spectral variability, with all three indices having low values, whereas land surfaces have at least one index with a relatively high value. The land variability probability is defined as one minus the maximum of the absolute values of the above three indices. The specific formula is as follows:

$$\begin{aligned}\text{Variability\_Prob} = 1 - max\ (&abs(NDVI),\\ &\text{abs}(NDSI), \text{and } Whiteness).\end{aligned} \tag{10}$$

The land cloud probability is calculated as the product of the temperature probability and the variability probability, with the temperature probability contributing more significantly for low-temperature pixels. A water pixel is identified as cloud when its cloud probability exceeds 0.5. A land pixel is identified as cloud when its cloud probability is greater than the 82.5th percentile of the cloud probabilities of clear-sky land pixels plus 0.2. In addition, if the land cloud probability exceeds 0.99 or the brightness temperature is 35°C lower than the lower bound of the clear-sky land temperature, these are used as supplementary criteria for omitted cloud pixels. The specific formulas are as follows:

$$\text{lCloud Prob} = lTemperature\ Prob * Variability\ Prob. \tag{11}$$

The overall cloud probability is combined with the potential cloud pixels (PCPs) from the first pass to finally generate the potential cloud layer, as shown in Equation (12):

$$\begin{gathered}\text{Potential Cloud Layer is true if} \\ (PCP \text{ (true) and } Water\ Test \text{ (true) and } wCloud_{Prob} > 0.5) \text{ or} \\ (PCP\text{(true) and } Water\ Test \text{ (false) and } lCloud\_Prob > Land\_threshold) \text{ or} \\ (ICloud\_Prob > 0.99 \text{ and } Water\ Test \text{ (false)}) \text{ or } (BT < T_{low} - 35).\end{gathered} \tag{12}$$

Finally, the Fmask algorithm performs spatial optimization using a 3×3 neighborhood window: if the number of cloud pixels within the central pixel's neighborhood is five or more, the central pixel is labeled as cloud. This processing improves the coherence and accuracy of cloud detection results, especially for cloud edges and thin cloud areas.

IV. RESULTS AND ANALYSIS

To validate the effectiveness of the proposed cloud detection algorithm, this study selected FY-4B/AGRI images at the full-disk scale and conducted a visual comparison between the cloud detection results and false-color composite images. The false-color composite was generated using Band3 (near-infrared channel), Band2 (red channel), and Band1 (green channel). This combination enhances the visual contrast among vegetation, water bodies, and clouds, facilitating the analysis of the improved cloud detection results.

The distribution of clouds over land is complex, comprising not only large, continuously distributed thick clouds but also fragmented thin clouds at the edges and small-scale cloud clusters. The cloud detection results over land are shown in Fig. 1. For thick cloud areas, the algorithm produces continuous and complete detections with clear cloud boundaries, which are highly consistent with the cloud contours observed in the false-color images. For thin cloud areas, the algorithm still detects most pixels, with only a small number of omissions occurring at the very thin edges where the clouds approach clear-sky conditions.

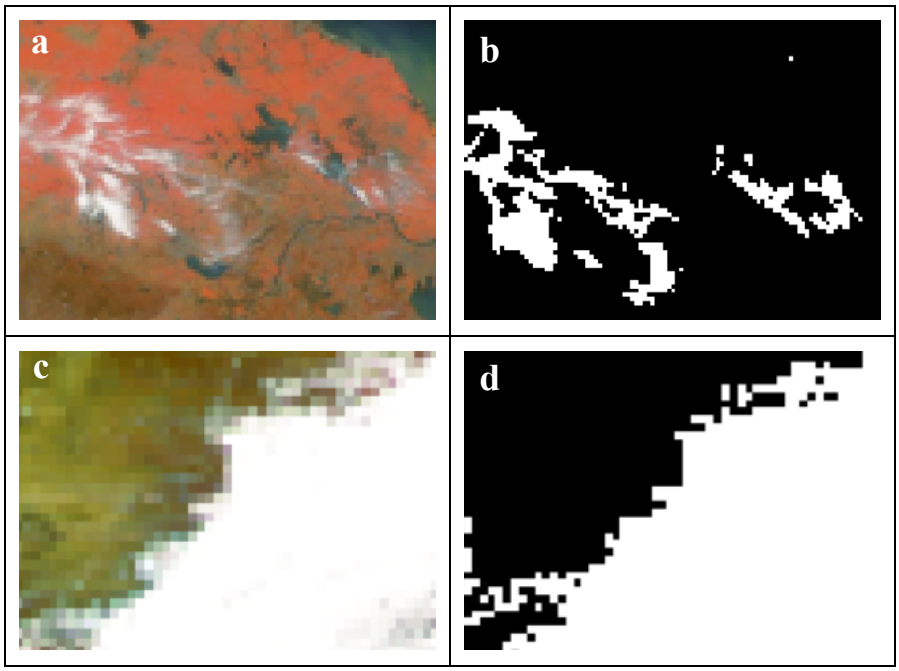

Fig. 1 Cloud detection results over land using the Fmask algorithm

Cloud distributions over water are also diverse, including not only large, continuously distributed thick clouds but also fragmented clouds of varying sizes and shapes. The cloud detection results over water are shown in Fig. 2. For thick cloud areas, the algorithm produces continuous detections with well-defined cloud boundaries, which are highly consistent with the cloud distributions observed in the false-color composite images. For fragmented cloud areas, the algorithm still detects most cloud pixels, with only a small number of omissions occurring in locally sparse cloud regions that are close to clear-sky water surfaces. Due to the low reflectance of water in the near-infrared band, the presence of clouds significantly increases the reflectance in this band. By combining temperature probability and brightness probability, the algorithm effectively eliminates interference from turbid water or cold water pixels.

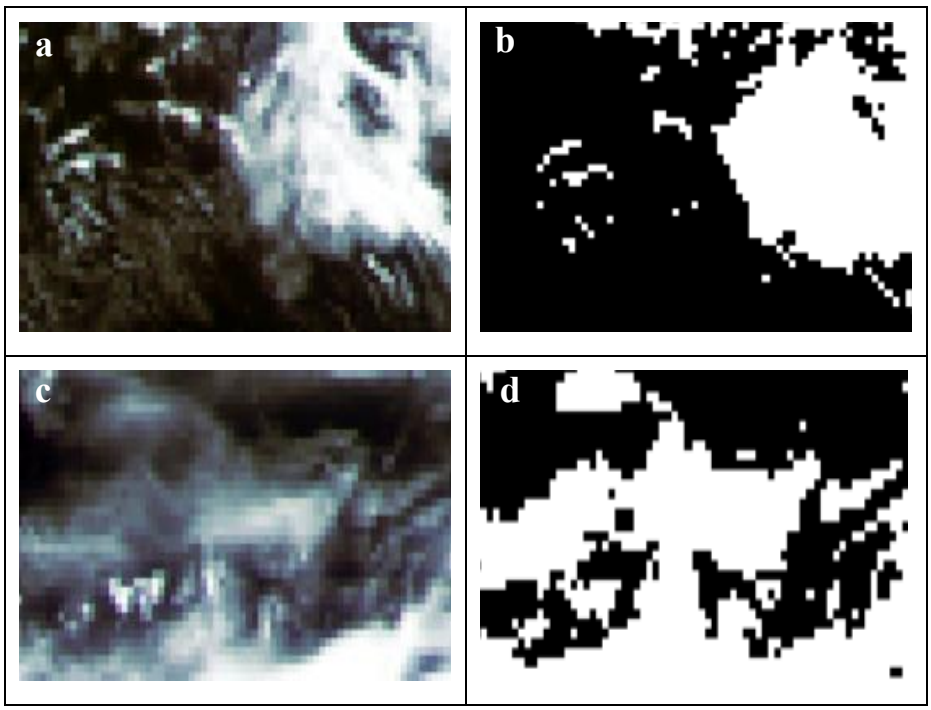

Fig. 2 Cloud detection results over water using the Fmask algorithm

To validate the applicability of the proposed algorithm at the full-disk scale, a cloud detection experiment was conducted using one FY-4B/AGRI full-disk image (acquired at 03:00 UTC on August 15, 2023). This image covers the Asia-Oceania region, including various land cover types such as ocean, land, and islands, with widely distributed cloud systems, making it suitable for comprehensive evaluation of the algorithm's detection performance. Fig. 3a shows the false-color composite image using Bands 3, 2, and 1, where white represents clouds; Fig. 3b shows the corresponding cloud detection results from the Fmask algorithm.

As shown in Fig. 3a, the cloud distribution in the full-disk image is complex, including thick clouds, thin clouds, fragmented clouds, and cloud clusters of varying scales. Fig.3b demonstrates that the Fmask algorithm maintains good detection performance at the full-disk scale: for thick cloud areas, the detection results are continuous and complete with clear boundaries; for thin cloud areas, although some omissions occur, the overall distribution is generally consistent with visual interpretation. No significant anomalies are observed in cloud detection over oceanic or land backgrounds, and the false detection rate is low. These results are consistent with the conclusions from the previous local-scale analyses, confirming the stability and operational applicability of the algorithm for full-disk images.

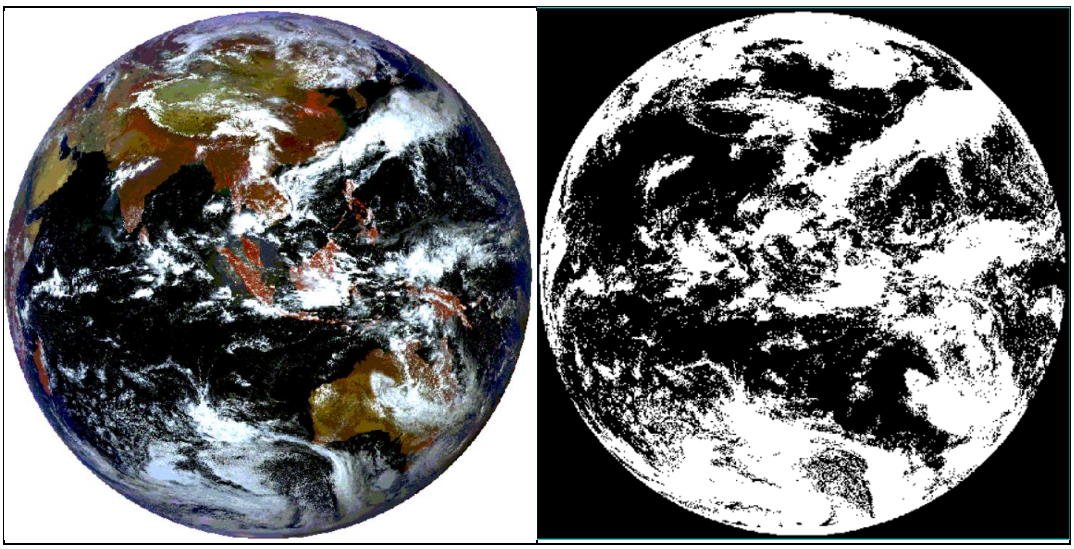

(a)FY-4B AGRI false-color composite image (b) Cloud detection result

Fig. 3 Cloud detection results for the full-disk image

V. CONCLUSION

In this study, a cloud detection method suitable for the 4 km resolution data of the Advanced Geosynchronous Radiation Imager (AGRI) onboard the FY-4B satellite was developed based on the core logic of the Fmask cloud detection algorithm. Through a systematic analysis of the spectral configuration of the AGRI sensor and the observational characteristics of geostationary satellites, adaptive improvements were made to the original algorithm that relied on specific bands (e.g., the green band). A multi-level spectral threshold discrimination system was proposed, including the basic test, whiteness test, HOT test, rock test, and water test. Cloud probability models were separately constructed for land and water, enabling pixel-level cloud identification and probabilistic assessment.

To validate the effectiveness and generalizability of the proposed algorithm, experiments were conducted using FY-4B/AGRI images covering different geographical regions and full-disk scales. The results show that the algorithm exhibits good detection performance over complex underlying surfaces, effectively identifying various cloud types such as thick clouds, thin clouds, and fragmented clouds, with clear cloud boundaries and a low false detection rate. The detection results over both land and water backgrounds are highly consistent with false-color composite images and thermal infrared images, demonstrating the robustness and reliability of the algorithm across multiple scenarios. Experiments on full-disk images further indicate that the algorithm has good scale adaptability and potential for operational applications.

In summary, the improved Fmask algorithm proposed in this study is well adapted to the characteristics of FY-4B/AGRI data, achieving high-precision and automated cloud detection, thereby providing reliable data support for subsequent applications such as quantitative retrieval from remote sensing imagery, climate change monitoring, and meteorological services. Future research can focus on further improving the detection capability for thin clouds, optimizing multi-temporal dynamic thresholds, and integrating deep learning methods to enhance the algorithm's generalization ability and detection accuracy under complex atmospheric and surface conditions.

REFRENCES

[1]. Myers, T.A., Scott, R.C., Zelinka, M.D., et al. [2021] "Observational constraints on low cloud feedback reduce uncertainty of climate sensitivity" Nature Climate Change, Vol. 11: pp.501-507.

[2]. Rosenfeld, D., Zhu, Y., Wang, M., et al. [2019] "Aerosol-driven droplet concentrations dominate coverage and water of oceanic low-level clouds" *Science*, Vol. 363(Issue 6427): pp.eaav0566.

[3]. Li, J., Wang, W.C., Dong, X., et al. [2017] "Cloud-radiation-precipitation associations over the Asian monsoon region: an observational analysis" Climate Dynamics, Vol. 49: pp.3237-3255.

[4]. Zhang, Y., Rossow, W.B., Lacis, A.A., et al. [2004] "Calculation of radiative fluxes from the surface to top of atmosphere based on ISCCP and other global data sets: Refinements of the radiative transfer model and the input data" Journal of Geophysical Research: Atmospheres, Vol. 109: pp.D19105.

[5]. Zhang, H., Huang, Q., Zhai, H., et al. [2021] "Multi-temporal cloud detection based on robust PCA for optical remote sensing imagery" Computers and Electronics in Agriculture, Vol. 188: pp.106342.

[6]. [Liu, C., Li, J., Li, B., et al. [2024] "Review of cloud property retrieval algorithms and product development for FY satellite optical imagers (Invited)" Acta Optica Sinica, Vol. 44: pp.29-42.

[7]. Liu, Y., Wu, C., Jia, R., et al. [2018] "An overview of the influence of atmospheric circulation on the climate in arid and semi-arid region of Central and East Asia" Science China Earth Sciences, Vol. 61: pp.1183-1194.

[8]. Roy, D.P., Wulder, M.A., Loveland, T.R., et al. [2014] "Landsat-8: Science and product vision for terrestrial global change research" Remote Sensing of Environment, Vol. 145: pp.154-172.

[9]. Irish, R.R., Barker, J.L., Goward, S.N., et al. [2006] "Characterization of the Landsat-7 ETM+ Automated Cloud-Cover Assessment (ACCA) Algorithm" Photogrammetric Engineering & Remote Sensing, Vol. 72: pp.1179-1188.

[10]. Zhu, Z. and Woodcock, C.E. [2012] "Object-based cloud and cloud shadow detection in Landsat imagery" Remote Sensing of Environment, Vol. 118: pp.83-94.

[11]. Zhu, Z., Wang, S. and Woodcock, C.E. [2015] "Improvement and expansion of the Fmask algorithm: cloud, cloud shadow, and snow detection for Landsats 4–7, 8, and Sentinel 2 images" Remote Sensing of Environment, Vol. 159: pp.269-277.

[12]. Qiu, S., He, B., Zhu, Z., et al. [2017] "Improving Fmask cloud and cloud shadow detection in mountainous area for Landsats 4–8 images" Remote Sensing of Environment, Vol. 199: pp.107-119.

[13]. Zhu, Z. and Woodcock, C.E. [2014] "Automated cloud, cloud shadow, and snow detection in multitemporal Landsat data: An algorithm designed specifically for monitoring land cover change" Remote Sensing of Environment, Vol. 152: pp.217-234.

[14]. Wei, B., Fu, L., Fan, F., et al. [2017] "A review of cloud detection methods in remote sensing images" Remote Sensing for Land & Resources, Vol. 29: pp.6-7.

[15]. Simonyan, K. and Zisserman, A. [2015] "Very Deep Convolutional Networks for Large-Scale Image Recognition" International Conference on Learning Representations: pp.1-14.

[16]. He, K., Zhang, X., Ren, S., et al. [2016] "Deep Residual Learning for Image Recognition" 2016 IEEE Conference on Computer Vision and Pattern Recognition (CVPR): pp.770-778.

[17]. Fu, H., Shen, Y., Liu, J., et al. [2019] "Cloud Detection for FY Meteorology Satellite Based on Ensemble Thresholds and Random Forests Approach" Remote Sensing, Vol. 11: pp.44.

[18]. Wei, J., Huang, W., Li, Z., et al. [2020] "Cloud detection for Landsat imagery by combining the random forest and superpixels extracted via energy-driven sampling segmentation approaches" Remote Sensing of Environment, Vol. 248: pp.112005.

[19]. Guo, X.X., Qu, J.H., Ye, L.M., et al. [2023] "FY-4A/AGRI cloud detection method based on naive Bayes" Journal of Applied Meteorological Science, Vol. 34: pp.282-294.

[20]. Li, Z., Shen, H., Cheng, Q., et al. [2019] "Deep learning based cloud detection for medium and high resolution remote sensing images of different sensors" ISPRS Journal of Photogrammetry and Remote Sensing, Vol. 150: pp.197-212.
[21]. Mahajan, S. and Fataniya, B. [2020] "Cloud detection methodologies: variants and development—a review" Complex and Intelligent Systems, Vol. 6: pp.251-261.
[22]. Chen, L., Xu, N., Wang, J.S., et al. [2025] "Fengyun satellites: From observation to quantitative application" Journal of Remote Sensing, Vol. 29: pp.1462-1479.
[23]. Luo, C.Y., Huang, X., Li, J.Z., et al. [2024] "Review of intelligent processing and typical applications of optical remote sensing data from Fengyun meteorological satellites (Invited)" Acta Optica Sinica, Vol. 44: pp.1800006.